Mon. Not. R. Astron. Soc. **000**, 1–14 (2009) Printed 11 February 2009 (MN LATEX style file v2.2)

Formation of Isolated Dwarf Galaxies with Feedback

Till Sawala[1⋆], Cecilia Scannapieco[1] and Simon White[1]
[1] *Max-Planck Insititute for Astrophysics, Karl-Schwarzschild-Strasse 1, 85748 Garching, Germany*

Accepted 2009 January 1. Received 2009 January 1; in original form 2009 January 1

ABSTRACT

We present results of high resolution hydrodynamical simulations of the formation and evolution of dwarf spheroidal galaxies. Our simulations start from cosmological initial conditions at high redshift. They include metal-dependent cooling, star formation, feedback from type II and type Ia supernovae and UV background radiation, with sub-grid recipes identical to those applied in a previous study of Milky Way type galaxies. We find that a combination of feedback and the cosmic UV background is necessary to explain the properties of dwarf spheroidal galaxies in isolation, and that their effect is strongly moderated by the depth of the gravitational potential. Taking this into account, our models naturally reproduce the observed luminosities and metallicities. The final objects have halo masses between 2.3×10^8 and 1.1×10^9 $M_\odot$, mean velocity dispersions between 6.5 and 9.7 kms^{-1}, stellar masses ranging from 5×10^5 to 1.2×10^7 $M_\odot$, median metallicities between [Fe/H] = -1.8 and -1.1, and half-light radii of the order of 200 to 300 pc, all comparable with Local Group dwarf spheroidals. Our simulations also indicate that the dwarf spheroidal galaxies observed today lie near a halo mass threshold around 10^9 $M_\odot$, in agreement with stellar kinematic data, where supernova feedback not only suffices to completely expel the interstellar medium and leave the residual gas-free, but where the combination of feedback, UV radiation and self-shielding establishes a dichotomy of age distributions similar to that observed in the Milky Way and M31 satellites.

Key words: cosmology: theory – galaxies: dwarf – galaxies: formation – galaxies: evolution – Local Group – methods: N-body simulations.

1 INTRODUCTION

Dwarf spheroidal galaxies are amongst the smallest and faintest known galactic systems, and at first sight, should be easy to understand. Their name indicates a simple morphology, they possess low rotation, little or no interstellar gas and no active star formation. Their stellar masses range from less than 10^4 to a few times $10^7 M_\odot$, which even at the more luminous end, makes them comparable to the brightest globular clusters. However, whilst all observed dwarf spheroidal galaxies contain at least a fraction of very old stars (Grebel 1997), this is where the similarities with globular clusters end. Spectroscopic surveys of individual stars in several dwarf spheroidal galaxies of the Local Group (e.g. Battaglia et al. 2006) have revealed surprisingly complex star formation histories, sometimes over several Gyrs, and at least in one case in multiple bursts (Koch et al. 2006, 2008).

About two dozen dwarf spheroidal galaxies have so far been discovered as satellites of the Milky Way, while estimates using luminosity functions corrected for completeness and bias predict the total number of faint satellites to be an order of magnitude higher (Tollerud et al. 2008). The known dwarf spheroidal galaxies in the Local Group reside in a variety of environments. There are a few near both M31 and the Milky Way, with distances of ~ 30 kpc and clearly within their hosts' dark matter haloes, as well as some remote objects like Cetus, which can be considered to have evolved in isolation (Castellani et al. 1996; Lewis et al. 2007).

It has been proposed for a long time (e.g. Faber & Lin 1983) and is now widely believed that the luminous component of dwarf spheroidal galaxies is not all there is to them. Their dynamics appear to be largely dark matter dominated, and measurements of stellar velocity dispersions (e.g. Koch et al. 2007; Walker et al. 2007; Mateo et al. 2008; Walker et al. 2009) indicate that they possess the highest mass-to-light ratios of any known galactic systems. Recent studies further suggest that despite the spread in luminosities, the total mass within the central 300 pc of the galaxies lies within a small range of around $10^7 M_\odot$ (Strigari et al. 2008).

It is also worth pointing out that in galaxy formation, small size can breed complexity. Shallow potential wells make these systems susceptible to both internal and external effects, such as violent supernova feedback, photoionization

⋆ E-Mail: till@mpa-garching.mpg.de

Table 1. Overview of Numerical Simulation Results

Label	f_s	$M_\star$ $[10^6 M_\odot]$	M_g $[10^6 M_\odot]$	M_{tot} $[10^6 M_\odot]$	$M_{0.3}$ $[10^6 M_\odot]$	$M_{1.8}$ $[10^6 M_\odot]$	$M/L_{0.3}$ $[[M_\odot/L_\odot]_V]$	$M/L_{1.8}$ $[[M_\odot/L_\odot]_V]$	$r_{1/2}$ [pc]	Δ age [Gyrs]	[Fe/H]	σ $[kms^{-1}]$
Simulations including feedback, UV radiation and self-shielding [a]												
1	0.368	0.55	0.099	233.8	8.48	79.0	129	555	244	1.13	-1.78	6.55
2	0.422	0.96	0.005	348.8	9.71	103.6	100	409	303	1.15	-1.76	7.26
3	0.464	2.10	0.009	466.1	11.5	125.7	39	223	226	2.51	-1.52	7.54
4	0.500	2.68	0.006	585.3	13.2	147.3	39	209	246	1.78	-1.54	8.12
5	0.531	3.94	0.14	701.8	14.8	165.9	26	156	212	1.21	-1.46	8.47
6	0.559	9.02	0.010	809.3	16.3	185.7	13	81	164	3.10	-1.12	8.62
7	0.585	10.02	0.005	922.3	17.9	203.5	13	80	171	3.23	-1.17	9.08
8	0.608	12.20	0.011	1042	17.9	218.5	12	71	190	3.30	-1.15	9.62
9	0.630	12.26	0.012	1162	21.0	235.1	14	76	181	3.21	-1.14	9.71
Simulations including UV radiation but no supernova feedback [a] [c]												
10	0.422	18.77	0.82	318.4	14.5	113.3	8	28	118	3.75	-0.71	-
11	0.531	99.50	9.64	645.6	27.0	216.5	6	14	160	6.46	-0.21	-
Simulations including feedback, UV radiation but no shielding[a]												
12	0.368	0.53	0.002	233.2	8.40	79.2	129	571	271	1.09	-1.78	6.39
13	0.422	0.99	0.005	351.7	10.3	103.8	98	407	289	1.11	-1.70	7.43
14	0.464	1.95	0.015	463.8	11.6	126.0	48	240	254	1.11	-1.52	7.67
15	0.500	2.75	0.19	582.7	13.5	148.1	38	201	248	1.16	-1.48	8.31
16	0.531	4.19	0.20	697.8	15.5	168.6	27	152	208	1.17	-1.38	8.40
17	0.559	6.91	0.55	811.2	16.6	187.6	17	105	186	1.14	-1.27	8.45
18	0.585	6.69	0.38	939.4	18.0	202.6	18	113	180	1.21	-1.29	9.12
19	0.608	9.31	0.58	1051	18.1	217.9	15	89	197	1.18	-1.32	9.38
20	0.630	9.65	0.65	1179	18.9	235.2	16	93	196	1.12	-1.31	9.74
Simulations including feedback but no UV radiation[a]												
21	0.368	1.38	0.077	229.6	9.08	79.24	36	202	180	7.96	-1.09	6.28
22	0.422	2.58	0.10	344.2	11.8	105.3	27	143	180	7.60	-1.03	7.11
23	0.464	4.58	0.08	458.4	13.4	128.6	19	105	178	5.49	-1.08	7.39
24	0.500	5.72	0.11	576.2	15.4	150.3	18	99	165	5.25	-1.06	8.17
25	0.531	7.14	0.098	685.9	16.3	158.5	16	90	171	4.53	-1.08	8.33
26	0.559	9.26	0.086	798.5	17.4	186.9	14	81	157	2.59	-1.12	8.75
27	0.585	10.95	0.064	909.0	17.5	204.3	13	76	169	3.66	-1.05	9.17
28	0.630	13.70	0.003	1147	20.1	236.9	12	69	181	3.71	-1.09	10.0
Simulations including feedback, UV radiation and self-shielding[b]												
29	0.422	0.59	0.008	338.7	6.88	104.1	157	737	375	1.21	-1.78	7.20
30	0.630	7.35	0.066	1141	15.5	235.4	18	133	245	2.62	-1.11	9.50

Notes: Col. 2: Scale factor (length) of the initial conditions relative to Hayashi et al. (2003), Col. 3: Stellar mass, Col. 4: Gas mass within 1.8 kpc, Col. 5: Halo mass (M_{200}), Col. 6: Dark matter mass within 0.3 kpc, Col. 7: Dark matter mass within 1.8 kpc, Col. 8: Mass-to-light ratio (V-Band) within 0.3 kpc, Col. 9: Mass-to-light ratio (V-Band) within 1.8 kpc, Col. 10: Half light radius (projected), Col. 11: Formation time interval containing 90 % of $M_\star$, Col. 12: Median stellar iron abundance, Col. 13: RMS stellar velocity dispersion

[a] Initial number of particles: 1.7×10^5 gas, 8.7×10^5 dark matter.
[b] Initial Number of particles: 1.21×10^6 gas, 2.83×10^6 dark matter.
[c] Simulations terminated at $z = 0.68$

and heating from the cosmic UV background, tidal interactions and ram-pressure stripping. All of these processes have the potential to shape the evolution of dwarf spheroidals, and to leave their mark on the star formation history and the chemical abundances, as well as on the morphology and dynamics of the final objects. They may explain some of the peculiar properties of dwarf spheroidals, including their very high mass-to-light ratios, and may also be responsible for the observed scaling laws (e.g. Woo et al. 2008). In this sense, the evolution of dwarf spheroidal galaxies can be considered an extreme case, but at the same time, an extremely good laboratory for astrophysical and cosmological processes (Marlowe et al. 1995). While the sensitivity to many parameters represents a considerable challenge for simulations, the large number of dwarf galaxies in the Local Group, together with the availability of high quality observational data also provides an unusually high number of constraints. Revaz et al. (2009 in prep.) exploit this fact by studying a large number of idealised models with non-cosmological initial conditions, which they can tune to reproduce the observed relations.

The number of dwarf galaxies observed in the Local Group is large, and continues to grow as new, 'ultra-faint' satellite galaxies are discovered (e.g. Martin et al. 2006; Chapman et al. 2008). Nevertheless, it is still much smaller than the total number of dark matter subhaloes found in

high-resolution simulations of spiral galaxy haloes in the standard ΛCDM cosmology (e.g. Klypin et al. 1999; Moore 1999; Diemand et al. 2007; Springel et al. 2008). This has become known as the 'missing satellites problem'. However, this is only an apparent discrepancy. It is removed when one accounts for the fact that not all subhaloes contain stars. Two possible mechanisms that can produce a number of visible satellite galaxies similar to that observed are the following. Perhaps many haloes were able to form a few stars initially, but the baryonic components of all haloes below some critical mass were subsequently destroyed by supernova feedback (e.g. Dekel & Silk 1986; Ferrara & Tolstoy 2000). Alternatively (or perhaps additionally) photoionization may have prevented star formation in the smallest haloes (e.g. Efstathiou 1992; Somerville 2002; Simon & Geha 2007). As dwarf spheroidals are the faintest known galaxies, a detailed understanding of their evolution should eventually reveal the influences of these two effects.

Examples of earlier numerical studies of the formation of dwarf galaxies include simulations by Read et al. (2006), Stinson et al. (2007) and Valcke et al. (2008). The latter two have investigated the collapse of gas clouds in dark matter haloes of constant mass. Both find evidence of prolonged and self-regulated star formation. However, while they do observe significant supernova-driven outflows, at a halo mass of $10^9 \mathrm{M}_\odot$, Stinson et al. find better agreement with dwarf irregular galaxies. Read et al. performed simulations of the formation of the first baryonic building blocks in a cosmological volume at high redshift. They confirm the importance of supernova feedback and UV heating (assumed to begin at $z = 13$) for removing the gas from the smallest haloes. However, they do not follow the evolution of the surviving objects to the present day, terminating their simulations at $z = 10$.

In this work, we model the formation and evolution of dwarf galaxies in isolation. We simulate a cosmological volume, in which the haloes grow from small density perturbations imposed at high redshift. Our fully dynamical model includes cooling, star formation, chemical enrichment and feedback, and we allow for exchange of material with the intergalactic medium. We use the same code, the same subgrid physics model and the same basic parameters employed by Scannapieco et al. (2008) to study the formation of Milky Way type disk galaxies, some 10^4 times larger in terms of stellar mass than the dwarf galaxies we consider here. We also include cosmological effects such as reionization. We do not study local environmental effects, which may play a role for the closest companion satellite galaxies to the Milky Way. The main questions that we will address are how it is possible that systems of such low luminosity and seemingly similar total masses undergo such complex and diverse star formation histories, why dwarf spheroidal galaxies have such high mass-to-light ratios, why they appear to follow certain scaling laws, and if their formation and evolution in a cosmological constant dominated Cold Dark Matter (ΛCDM) universe can be explained by a consistent physical model. In Section 2, we present the computational methods which we have used and our choice of initial conditions. Section 3 follows with a presentation of the results of our simulations in broad terms, and in particular the influence of supernova feedback and the UV background radiation. In Section 4, we focus on the observed scaling laws, and present the dependence of our results on model parameters. We conclude with a summary where we discuss the achievements and shortcomings of the simulations in Section 5, and look forward to our future work.

2 METHODS

2.1 Computational Methods

The simulations presented here have been performed using the Tree-PM code GADGET-3 (Springel 2005; Springel et al. 2008), which includes gravity and smoothed particle hydrodynamics. As an extension, metal-dependent cooling, star formation, chemical enrichment and energy injection from type II and type Ia supernovae have been implemented in the multiphase gas model of Scannapieco et al. (2005, 2006). This model has previously been used to study the effect of feedback on galaxy evolution in general terms (Scannapieco et al. 2006) and the formation of disk galaxies in particular (Scannapieco et al. 2008, 2009). Star formation is implemented so that gas particles can spawn, or be converted into, star particles, subject to certain constraints. We require the gas particle to be in a region of convergent flow. We impose a physical density threshold of $n_\mathrm{H} = 0.1\mathrm{cm}^{-3}$ following Kennicutt (1998), as well as a threshold of $\rho_\mathrm{g}/\overline{\rho_\mathrm{g}} \geqslant 57.7$ on the local gas overdensity (where $\overline{\rho_\mathrm{g}}$ is the global mean density) to ensure that star formation takes place only in virialised regions at high redshift. In this model, the local star formation efficiency is regulated by a single efficiency parameter $c_\star$, so that the star formation rate is given by

$$\frac{d\rho_\star}{dt} = c_\star \frac{\rho_g}{t_\mathrm{dyn}}$$

where t_dyn is the local gas dynamical time.

Each star particle thus produced contains a single stellar population, whose metallicity is inherited from the parent gas particle. For simplicity, we assume a Salpeter initial mass function (Salpeter 1955). We calculate the luminosities at any given time using the stellar evolution model of Bruzual & Charlot (2003). Averaged over the entire populations, the metal- and age-dependent stellar mass-to-light ratios in the V-Band obtained in this way lie between $2 - 4\mathrm{M}_\odot/\mathrm{L}_\odot$ in our simulations. For each star particle, we determine the rate as well as the yields of supernovae type II and type Ia, which we assume to provide 10^{51} erg of thermal energy per event. Chemical yields are calculated following Woosley & Weaver (1995) and Thielemann et al. (1993) for type II and type Ia, respectively. The energy and metals are injected into the two phases of the interstellar medium. Decoupling of the cold and dense phase (which satisfies the criteria for star formation set above), and the hot and dilute phase, prevents the immediate loss of energy via radiative cooling. A full description of the feedback model is contained in Scannapieco et al. (2005) and Scannapieco et al. (2006). In the simulations where we include a cosmic UV background, we follow the model of Haardt & Madau (1996).

2.2 Initial Conditions

All simulations are performed in the context of a ΛCDM cosmology, with $\Omega_\Lambda = 0.7$ and $\Omega_\mathrm{m} = 0.3$. We use a set of initial

conditions of varying resolution, based on pure dark matter simulations of isolated haloes by Hayashi et al. (2003). The initial conditions on which our simulations are based (labeled D1 by Hayashi et al.) were selected from their set of dwarf haloes in order to yield an object whose high redshift progenitors fill a compact region in space, enabling us to limit the high resolution region to a small fraction of the total volume, whose (unscaled) side length is 35.25 h^{-1} Mpc. Our resimulations start at redshift $z_i = 74$ with density fluctuations for a present value of $\sigma_8 = 0.9$. To the dark matter, gas particles were added at a rate of $\Omega_\mathrm{b} = 0.04$ and $\Omega_\mathrm{DM} = 0.26$.

In order to change the mass of the final object, we have scaled the initial conditions at constant density, to give final halo masses between 2.33×10^8 and 1.18×10^9 $h^{-1}\mathrm{M}_\odot$. We have also performed simulations of varying particle numbers (up to 2.83×10^6 for dark matter and 1.12×10^6 for gas). The gravitational softenings for each particle type were fixed to 1/10th of the respective mean interparticle separation in comoving coordinates in the initial conditions and limited, in physical coordinates, to $\sim 1/5$th of the mean separation within the collapsed haloes. This allowed a spatial resolution typically below 100 pc (depending on the scale and the number of particles). Haloes were identified using a friends-of-friends method with a linking length of 0.2. In each case, over a hundred small haloes with 32 particles or more were formed in the simulated volume, and depending on the choice of parameters of the baryonic physics model, several of them formed stars. However, in each case we limit our analysis to the most massive one, for which the effective resolution is highest. We have made tests to confirm the scale-free behaviour of the pure dark matter simulations. We find that in all cases, the dark matter profiles are well-fitted by a Navarro, Frenk and White (NFW) model, down to the resolution limit. Note that all our simulations have the same assembly history, apart from resolution effects. This means that we cannot say anything about the scatter in properties expected among similar mass haloes. On the other hand, differences between our various simulations must therefore be due entirely to differences in the assumed physics or the numerical parameters. Cosmic variance plays no role.

3 FORMATION AND EVOLUTION

We find that the evolution of the dwarf galaxies that we simulate is strongly effected both by supernova feedback and by the UV background radiation. It is the combination of these two effects that shapes the evolution of the galaxy. We begin this section by showing the evolution of a typical dwarf galaxy up to the present time, including all the different effects that play a role, but focusing on the global picture. We then try to disentangle the effects of feedback and UV radiation, and look in more detail at how they influence the evolution.

3.1 Time Evolution

Figure 1 illustrates different stages in the evolution of a proto-galaxy (labeled simulation 16 in Table 1) together with its environment. The top row shows the position of dark matter, gas and star particles. The scale of the panels is kept constant in physical coordinates with a side length of 20 kpc, hence the volume displayed shrinks in terms of comoving coordinates and the view zooms in on the central galaxy as the redshift decreases from left to right. In the first two columns, the filamentary structure of the environment is still recognisable, together with a number of smaller haloes that have accumulated gas, but not yet begun star formation. The bottom row shows the distribution of gas particles on the density-temperature plane, both within and outside of the most massive halo.

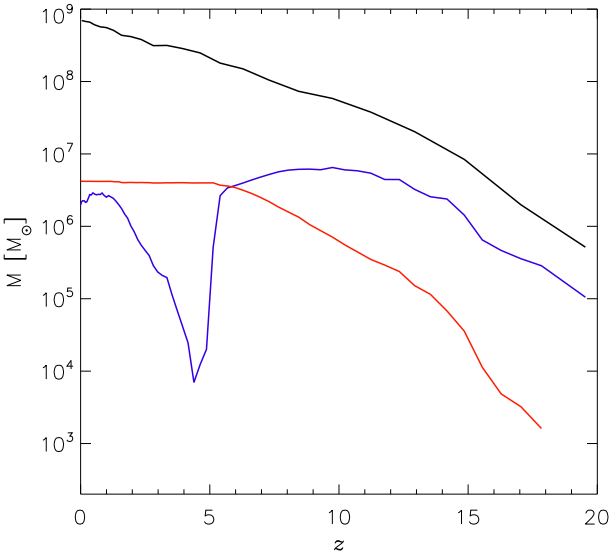

Figure 2. Evolution of the dark matter mass (in black), gas mass (in blue) and stellar mass (in red) as function of redshift, for a simulation including star formation, supernova feedback and a cosmic UV background, without self-shielding. Parameters of this simulation, and the status at $z = 0$ are summarised in Table 1 (simulation 16).

As the halo forms, gas begins to fall in, contracts and gets heated. At a temperature of 10^4 K, radiative cooling becomes so efficient that the gas can contract essentially isothermally, until the central density reaches the threshold for star formation, as described in Section 2.1. At $z = 12.3$, which corresponds to the leftmost column of Figure 1, the first stars have already formed in the central object, and supernovae of type II have started heating the gas, already pushing some of it out. This is visible also in the bottom row of Figure 1, where the gas particles that start appearing to the right of 10^4 K, which indicates that they have been heated by supernovae, are no longer bound to the halo.

The total masses of the three components; dark matter, gas and stars identified as belonging to the halo by a friends-of-friends algorithm, are shown as a function of time in Figure 2. Star formation in the galaxy continues for about one Gyr, as more gas gets accreted and cools, whilst supernovae of both type II and type Ia continue to expel the interstellar medium. Ejection and heating balance accretion and cooling at $z = 9$, and the star formation rate peaks at $z = 8$. By redshift $z = 6$, the star formation rate has already decreased by a factor of two from its peak value of $3 \times 10^{-1}\mathrm{M}_\odot$ yr^{-1} due to feedback.

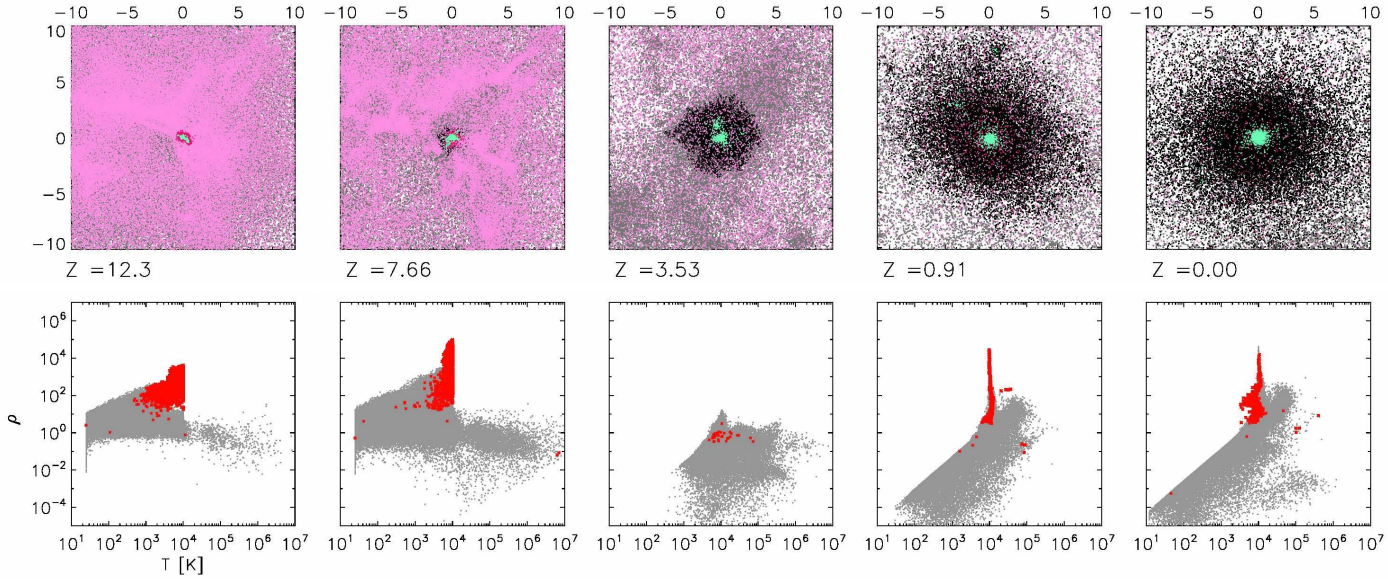

Figure 1. Top row: Spatial distribution of particles of different types at different redshifts of simulation 16 in Table 1. Dark matter particles are shown in black (or grey), gas particles in red (or purple), depending on whether they are bound to the object in the centre, or whether they are part of other haloes or the intergalactic medium. Star particles are shown in green. Bottom row: Temperature and density of gas particles. Red dots indicate gas that is bound to the central halo, while grey dots are for particles in all other parts of the simulated volume. Both supernova feedback and UV radiation are included in this simulation. It can be seen that the central halo is almost gas-free at redshift $z = 3.5$, due to the combined effect of feedback and the UV background. Feedback heats the gas and blows some of it out during the early stages of the evolution. After redshift $z = 6$, UV radiation heats the remaining gas above the haloes virial temperature, quickly removing it from the halo, and also heats the intergalactic medium. Some gas falls back to the main halo at later times, but does not lead to significant amounts of star formation. Smaller haloes without star formation, and hence not subject to feedback, also lose their gas due to the UV radiation.

At $z = 6$, the UV background suddenly switches on. In this particular model, it is sufficient to heat the remaining gas above the virial temperature of the halo in a very short time, resulting in its expulsion, and a sharp end to star formation. Some gas falls back at a later stage, but does not reach sufficient density for star formation.

It can be seen in Figure 2 that the dark matter haloes in our simulations continue to grow over time through accretion and minor mergers. It is worth noting that throughout the period of star formation, from the onset around redshift $z = 16$ to the end shortly after redshift $z = 6$, the halo mass is several times smaller than the final value, which might be observed today. This contributes to the high efficiency of the winds in our models. It also suggests that the impact that supernova feedback might have had during the history of a particular dwarf galaxy not only depends on its 'mass' as it is presently observed, but also on the co-evolution of its star formation and the assembly of its halo at earlier times. This fact is taken into account explicitly in semi-analytic models like that of Ferrara & Tolstoy (2000), but it is overlooked in non-cosmological simulations that assume collapse in a static potential.

In our simulations, the halo continues to grow unperturbed up to $z = 0$. This is not necessarily true for haloes of satellite galaxies, which may have experienced truncation upon infall (Nagai & Kravtsov 2005). However, at least according to our models, it is likely that star formation would have finished before a typical infall redshift of $z \sim 1$ or below (Li & Helmi 2008). While we therefore do not expect environmental effects to significantly alter the stellar population, they may further skew the correspondence between observed halo masses today, and gravitational potential in place at the epoch of star formation. We also assume that the late infall of gas, leaving in some cases a small amount of gas at $z = 0$, in disagreement with observations, would be different in the Local Group environment.

3.2 The Effect of Feedback

As we have seen, feedback from supernovae is sufficient to expel gas from the shallow potential wells of forming dwarf-galaxies, and it is responsible for regulating star formation at least up to redshift $z = 6$. By performing test simulations without a UV background, we find that supernova feedback alone can blow out all the remaining gas before redshift $z = 0$ even in the absence of photoelectric heating, albeit at a much slower rate, resulting in a larger number of intermediate age stars. Even in this case, only between 3% and 6% of the total amount of gas ever bound to the halo gets turned into stars, depending on the mass of the object. Most of the gas still escapes to the intergalactic medium, enriching it with metals.

In simulations without thermal feedback (simulations 10 and 11 in Table 1), the picture is drastically different. Not only is the star formation more efficient during the early stages, the interstellar gas also becomes so dense that all

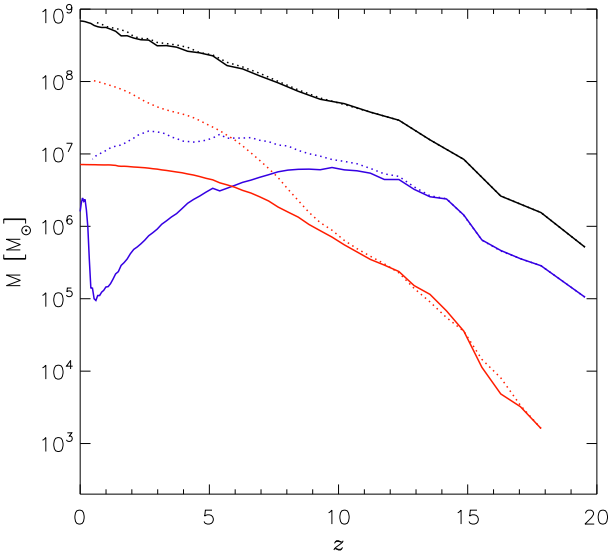

Figure 3. Evolution of the dark matter mass (in black), gas mass (in blue) and stellar mass (in red) as function of redshift. Initial conditions are identical to those shown in Figure 2, but the evolution is different. The solid lines shown here are for simulation 25, where feedback is the only source of heating, whereas the dotted lines are for simulation 11, that includes UV radiation from redshift $z = 6$ but no feedback. In the first case, feedback alone is sufficient to remove most of the gas, but more slowly compared to Figure 2. The decline in the gas mass in the second case is solely due to consumption and conversion to stars. Furthermore, without feedback, the UV background present from $z = 6$ has almost no effect on the pair of dotted lines.

effects of the UV background radiation are eliminated due to very efficient cooling. The result is a system of large stellar mass (up to $10^8 M_\odot$ in the case of simulation 11, compared to $4\times10^6 M_\odot$ for the same initial conditions run with feedback), low mass-to-light ratio, high metallicity, an abundance of young stars, and a high gas content. All these properties are incompatible with observations of dwarf spheroidals.

Figure 3 illustrates two 'incomplete' scenarios. We show the evolution of dark matter, gas and stellar mass, for simulation 25, where feedback is the *only* source of thermal energy, and for simulation 11, where UV radiation is included, but stellar feedback is ignored. They can be compared with Figure 2, where the combined effect of supernova feedback and UV background radiation are shown for simulation 16. All three simulations have identical initial conditions and numerical resolution. While the growth of the dark matter mass appears unaffected by the baryonic physics, the red and blue lines, which indicate the stellar and gas mass, respectively, show large differences. The outflow induced by feedback causes the solid blue line representing the gas mass in Figure 3 to peak at about $z = 9$ and decline thereafter, as in Figure 2. The star formation rate (not shown) also declines and the solid red line, representing the total stellar mass, increases ever more slowly, reaching $7\times10^6 M_\odot$ at redshift $z = 0$. In contrast, the dotted blue line in Figure 3, which represents the gas mass without feedback, shows no decline at high redshift. The total baryon fraction of the halo stays constant at around 1/6th, indicating that the late decline of the gas mass is due solely to consumption by star formation. It is worth reiterating that this simulation includes the full UV background (see Section 3.3), without self-shielding (see Section 3.4). Contrary to the results of Figure 2, we find that when thermal feedback is ignored, the UV radiation has no effect either. The gas density is so high that the gas can cool fast enough to balance any heating due to the cosmic background. We conclude that feedback is necessary to shut down star formation in those haloes massive and dense enough to cool and begin forming stars.

As shown in Table 1, the mean one-dimensional velocity dispersions in each galaxy resulting from our simulations are in the range of 6.5 to 9.7 kms^{-1}. This is comparable to the observed range of 7 to 10 kms^{-1} for six of the seven 'classical' Local Group dwarf spheroidals in the sample of Walker et al. (2007). The one exception, Fornax, has a velocity dispersion of about 12 kms^{-1}. Its stellar population, which includes several globular clusters, is more spatially extended, and its stellar mass is also slightly higher than that of the most luminous galaxy in our simulations. At the faint end, an extrapolation of our results might also be consistent with the corresponding values of the eight ultra-faint Milky Way satellites presented in Simon & Geha (2007), which have velocity dispersions between 3.3 and 7.6 kms^{-1}.

We also investigated the influence of supernova feedback on the shape of the dark matter distribution. It is still an open question whether flat cores, rather than the cusps predicted by dissipationless cold dark-matter models exist in the central regions of dwarf galaxy haloes. While for a stellar system with uniform mass-to-light ratio, the shape of the gravitational potential can be uniquely determined from the observed velocity dispersion and surface brightness profiles, in the case of the highly dark-matter dominated dwarf spheroidal galaxies, the unknown mass-to-light ratios result in a degeneracy between the gravitational potential variation and the velocity anisotropy (Dejonghe & Merritt 1992). The same data, when analysed with different anisotropy assumptions, can therefore result in different density profiles, and as van den Bosch & Swaters (2001) and Evans et al. (2008) have shown, the stellar kinematics of dwarf spheroidal galaxies are generally not sufficient to distinguish between cored and cusped profiles. Nevertheless, reports of central-density cores in dwarf galaxies (e.g. Carignan & Beaulieu 1989; de Blok et al. 2001; Łokas 2002) have been considered as evidence for warm dark-matter (e.g. Moore 1994). Within the framework of ΛCDM, numerical simulations by Navarro et al. (1996), Read & Gilmore (2005) and others have suggested that cores of kpc scale may form as a result of rapid ejection of large amounts of baryonic matter by supernova feedback. Our simulations fail to fulfil these requirements in two ways. The ejection of gas is not sufficiently rapid (which would also be difficult to reconcile with the observed age-spreads), and our dark matter haloes continue to grow after star formation and supernova rates have peaked, instead of simply settling to an equilibrium configuration. As a result, we do not observe the formation of cores in our runs with feedback. The final dark matter density distributions can be described by NFW-profiles up to the resolution limit.

3.3 The UV Background

Quasar spectra indicate that the universe has been fully ionised from about redshift $z = 6$ (Fan et al. 2002). This prompted us to include a background of UV radiation in our model, which we have adopted from Haardt & Madau (1996). The question of whether dwarf galaxies survive the cosmic reionization epoch has been an intense area of study (e.g. Kitayama et al. 2002; Susa & Umemura 2004; Hoeft et al. 2006). In hydrodynamical simulations, Hoeft et al. (2008) find that UV heating reduces the baryonic fraction in galaxies below a characteristic total mass, $6 \times 10^9 M_\odot$. However, Grebel & Gallagher (2004) found no clear signature of a widespread impact from reionization in their analysis of age distributions of nearby dwarf galaxies.

In Figure 4, we show the evolution of a system that includes feedback but no UV radiation (simulation 25 in Table 1), a simulation otherwise identical to simulations 16, which is shown in Figures 1 and 2. The most obvious difference to note when comparing the two sets of figures is in the low density regions of the intergalactic medium, where heating by the UV background is most effective.

We find that all haloes that are not massive enough to accrete sufficient gas to form stars before $z = 6$ subsequently lose their gas when the effects of photoelectric heating are included. This supports the idea that reionization establishes a lower mass threshold for dwarf galaxy haloes, and so provides part of the solution to the 'missing satellites problem'. However, we do not observe star formation in these haloes, even when UV radiation is ignored, most likely due to inefficient cooling as a result of insufficient resolution.

With respect to those objects massive enough to acquire dense, star-forming gas at high redshift, we have already shown that the UV background alone is not sufficient to shut off star formation at $z = 6$. Feedback is required in order to make the gas diffuse and to reduce its radiative cooling efficiency. However, when this requirement is met, the UV background radiation has a strong influence on the star formation timescale. While the difference in total stellar mass varies from 30 % for the largest system to a factor of three for the smallest system we have studied, this alone may not be enough to be discriminatory when comparing mass-to-light ratios with observations. However, a substantial difference is also found in the age and metallicity distributions. When star formation continues beyond reionization, many intermediate age stars with high metallicities are formed, and, as can be seen in Table 1, this causes the median metallicity to saturate around [Fe/H] $= -1.1$ when the UV background is ignored. Moreover, while properties such as the total stellar mass and metallicity also depend on the initial mass and (less strongly) on other parameters of the model (see Section 4), the age distribution of the stars does not. In all cases with UV radiation, the termination of star formation at $z = 6$ results in a narrow age distribution, as can be seen in Figure 5, while in all cases without the UV background, there is a pronounced intermediate-age tail. This is significant, because there appear to be examples of both types of galaxies in the Local Group (Grebel & Gallagher 2004). We have tested the dependence on the overall UV intensity, and found qualitatively similar results when we decreased it by up to a factor of 10 from the Haardt & Madau (1996) level. Furthermore, while there may be local variations in the UV background, particularly at higher redshift and from sources other than quasars (e.g. Ciardi et al. 2003), the mean free path of UV photons in the intergalactic medium is on the order of tens of Mpc (Bolton et al. 2004), which seems to rule out the possibility that the observed variation in star formation histories can be attributed solely to small-scale variations of the background radiation level.

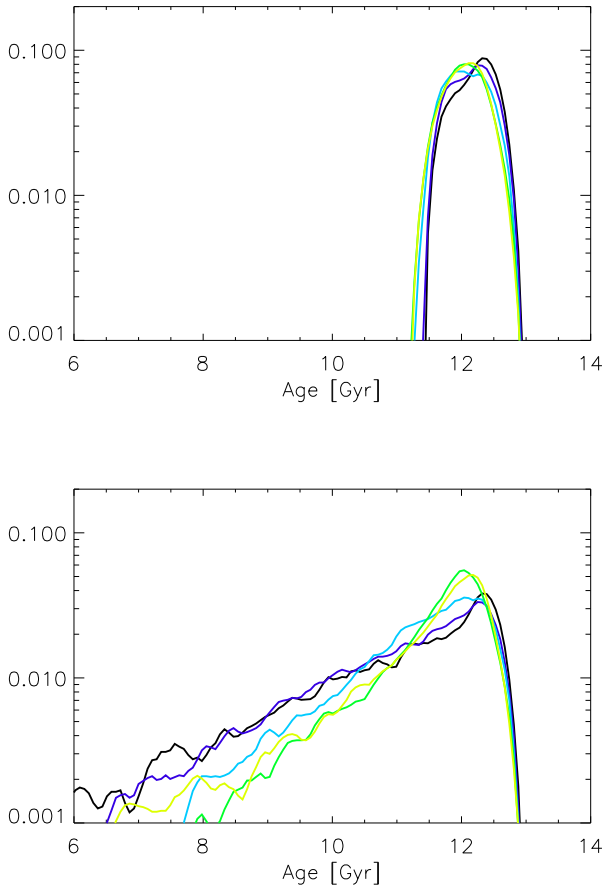

Figure 5. Distribution of stellar ages in Gyr. Simulations of the same halo mass are shown in the same colour, brighter colours indicate higher mass. The two panels show the results of simulations including a UV background, on top, and without a UV background, on the bottom.

3.4 Self-Shielding

We have also performed simulations where we approximate the effects of self-shielding of the dense interstellar medium against the UV background. While we do not include radiative transfer in these simulations, we use a threshold on the density of neutral hydrogen (HI) gas of $n_{HI} = 1.4 \times 10^{-2} cm^{-3}$, following the results of Tajiri & Umemura (1998). Including this effect leads to an interesting dichotomy. At the more massive end, as shown in the bottom row of Figure 6, the evolution in the central object proceeds almost as in the case with no UV background, while at the low mass end, as shown in the top row of the same figure, the evolution is similar to the case with UV heating but no shielding.

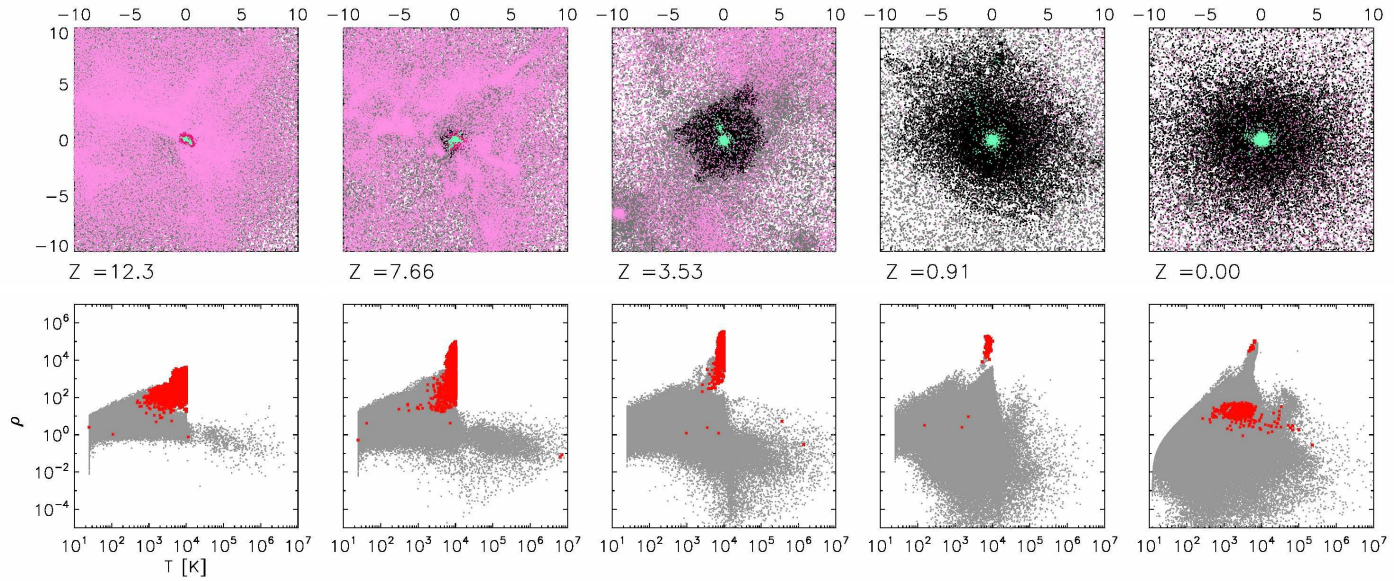

Figure 4. Top row: Spatial distribution of particles of different types at different redshifts of simulation 25 in Table 1. Dark matter particles are shown in black (or grey), gas particles in red (or purple), depending on whether they are bound to the object in the centre, or whether they are part of other haloes or the intergalactic medium. Star particles are shown in green. Bottom row: Temperature and density of gas particles. Red dots indicate gas that is bound to the central halo, while grey dots are for particles in all other parts of the simulated volume. The simulation is identical to the one shown in Figure 1, but contains no UV radiation. While the system still looses almost all its gas, this happens more slowly, and the stellar mass continues to grow beyond redshift $z = 6$. The most noticeable difference, however, is in the smaller haloes (10^6 $M_\odot$ or less), which did not form stars early on, and which would now be able to retain their gas.

Figure 7 shows the star formation rates over time for six simulations: the two simulations with self-shielding discussed above, and their equal-mass counterparts without shielding, both with and without a UV background. The evolution in each set of three simulations is identical up to redshift $z = 6$, when the onset of the UV background quenches star formation in both unshielded cases. When shielding is included it has no effect in the low-mass case, where the star-formation rate shows a similar, sharp decline. In contrast, in the high-mass case, the star formation rate with shielding closely follows that in the corresponding simulation without UV radiation.

The age distributions shown in Figure8 reflect this. Systems with lower mass only have small age spreads resulting from a single burst, comparable with the results without shielding shown in Figure 5 (matching colours indicate equal masses). Higher mass objects possess intermediate age tails, similar to the result without a UV background.

Again, we find that while it is the response of the interstellar medium to the UV radiation that ultimately splits the two scenarios, it is the effect of feedback prior to reionization that is at the root of this dichotomy. In the low-mass case, feedback dilutes the gas more efficiently prior to reionization, and thereby prevents it from self-shielding. In the high-mass case, the gas in the centre is still dense enough to become self-shielding and to prevent a blow-away.

While the approximation of self-shielding is very crude, and should be confirmed by more detailed analysis with full radiative transfer, it is interesting that the critical gas density that determines whether galaxies form stars after reionization appears to lie just at the right level to allow the formation of both kinds of dwarf spheroidal galaxies in simulations which include supernova feedback. On the basis of these arguments, it appears that the inclusion of cosmic reionization and a UV background with the possibility of self-shielding is the physically correct assumption. In the subsequent analysis, we continue to use the Haardt & Madau (1996) model, together with our approximation for self-shielding. We note, however, that the environment in which our galaxies form is different to that of the Local Group. This may play an additional role in the star formation history. Possible environmental effects include not only a local variation in the UV background, but also other mechanisms for removing gas, or reducing its density in satellite galaxies. While the removal of gas, by ram pressure stripping, for example, could halt star formation directly, our results indicate that an indirect mechanism might be just as efficient, if it makes the gas susceptible to evaporation after $z = 6$. That such environmental effects play a role is supported by the observation that dwarf spheroidals close to the centre of the Milky Way tend to have fewer intermediate age stars than those further out, although this trend is less clear for the M31-satellites (Grebel 1997).

4 EXPLORING THE PARAMETER SPACE

Even though our model is physically motivated, it contains several physical parameters which cannot be determined ab initio in our simulations. We have therefore explored a range of variables that have a direct physical significance, some of

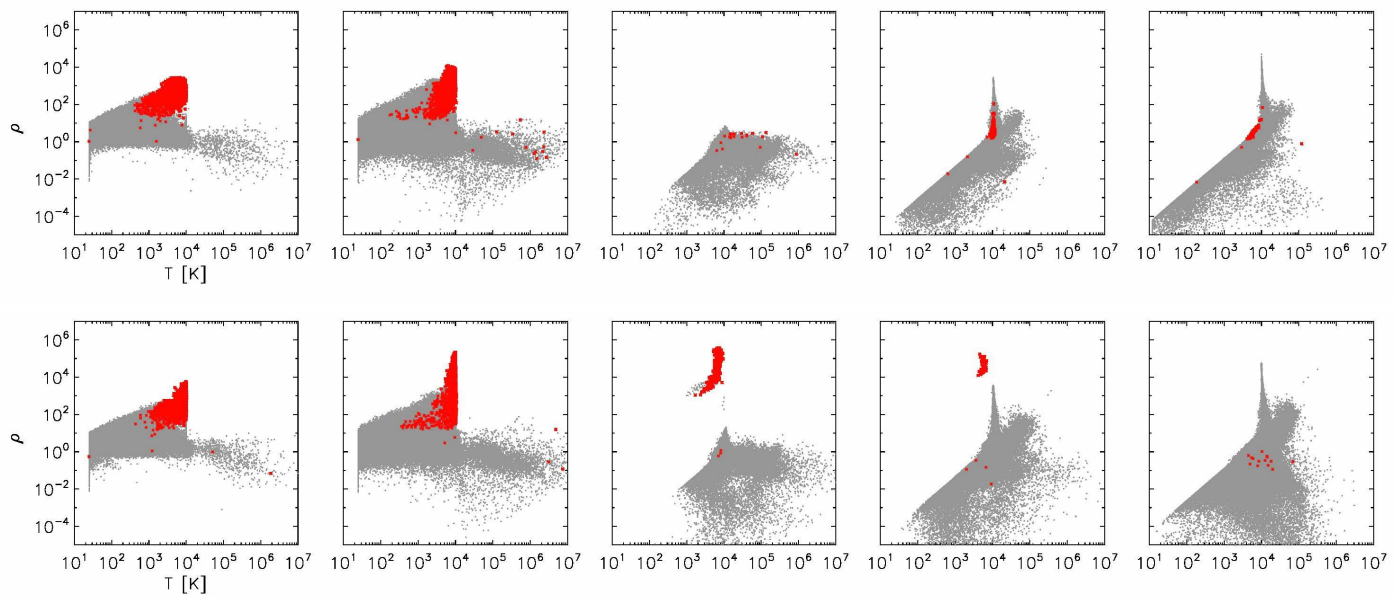

Figure 6. Temperature and density of gas particles. Red dots indicate gas that is bound to the central halo, while grey dots are for particles in all other parts of the simulated volumes. Results from two simulations of different mass illustrate the effect of self-shielding. Simulation 2, shown on top, has a final halo mass of $3.5 \times 10^9 M_\odot$, while simulation 7, shown below, has $9.2 \times 10^8 M_\odot$. Both simulations include supernova feedback and UV radiation, similar to those shown in Figure 1. At redshift $z = 7.6$, prior to reionization, the higher mass simulation has been able to keep a larger amount of dense interstellar gas in the centre, whereas feedback has caused the gas in the lower mass galaxy to be more diffuse. At redshift 3.5, the gas in the lower mass galaxy has been lost, while the higher mass galaxy has kept its high density gas, allowing it to form stars up to redshift $z = 1$. In both cases, black points, associated with the IGM and smaller haloes, are distributed similarly to the case with UV heating but no shielding in Figure 1, indicating that self-shielding is not efficient in these low density environments.

which we hope to constrain by comparison with observations, and others that may simply help to explain the variation amongst the observed systems.

4.1 Total Mass: Scaling Relations

Measurements of stellar kinematics of the Local Group dwarf galaxies have recently revealed a striking similarity in the inferred virial mass contained within the central 300 pc. It is consistent with a common value of $10^7 M_\odot$ over several orders of magnitude in luminosity (Strigari et al. 2008). This suggests that dwarf spheroidals reside in similar dark matter haloes. Why then do they have such a large variation in stellar mass?

Some of the effects of the depth of the potential well have already been described in Sections 3.4 and 3.3 on the UV background, reflecting the fact that no parameter can really be studied in isolation. In this section, we look at the series of simulations that includes all of the physical processes: cooling, star formation, feedback, UV radiation and self-shielding, but focus on a comparison with the observed scaling relations. We have scaled the initial conditions at constant density, which results in final virial masses between 2.3×10^8 and $1.2 \times 10^9 M_\odot$, and masses within 300 pc between 0.9×10^7 and $1.8 \times 10^7 M_\odot$, similar to those obtained by Strigari et al.. We nevertheless find a surprisingly large variation in stellar mass, luminosity, central mass to light ratio and metallicity, as summarised in Table 1. The final stellar masses range between 5.5×10^5 and $1.2 \times 10^7 M_\odot$, whilst the median iron abundance ranges from [Fe/H] = −1.78 to −1.12. In Figure 9, we show that this is sufficient to reproduce the well-known mass-metallicity relation (e.g. Mateo 1998) of dwarf spheroidals. We compare the results from our simulations, shown in red, to those of 14 'classical' Local Group dwarf spheroidals as given by Woo et al. (2008), overplotted in black. We find that there is good agreement, both in the range of metallicities obtained, as well as in the slope of the relation. We also show the distributions of metallicities of individual star particles per galaxy in Figure 10. Comparing this with observed distributions, e.g. by Helmi et al. (2006), we find an overabundance of both metal-rich and metal-poor stars for a given median metallicity, which we attribute to a lack of metal-mixing in the interstellar medium of our simulations.

In Figure 11 we compare the same set of simulations to observed Milky Way satellite galaxies in terms of their luminosities and mass-to-light ratios. The observational sample is identical to the one used by Strigari et al. (2008), and comprises 8 'classical' dwarf spheroidals, as well as 10 of the newly-discovered ultra-faint galaxies (Willman et al. 2005; Belokurov et al. 2007). While the observed galaxies span an even larger range in luminosity than the ones we have simulated, we find a similar, tight inverse correlation between luminosity and mass-to-light ratio. Whereas Strigari et al. find only a very weak dependence $M_{0.3} \propto L^{0.03 \pm 0.03}$, our relation is somewhat steeper at $M_{0.3} \propto L^{0.24}$. This is still a remarkably weak dependence, and it allows us to reproduce a large range in luminosity with an $M_{0.3}$ mass that

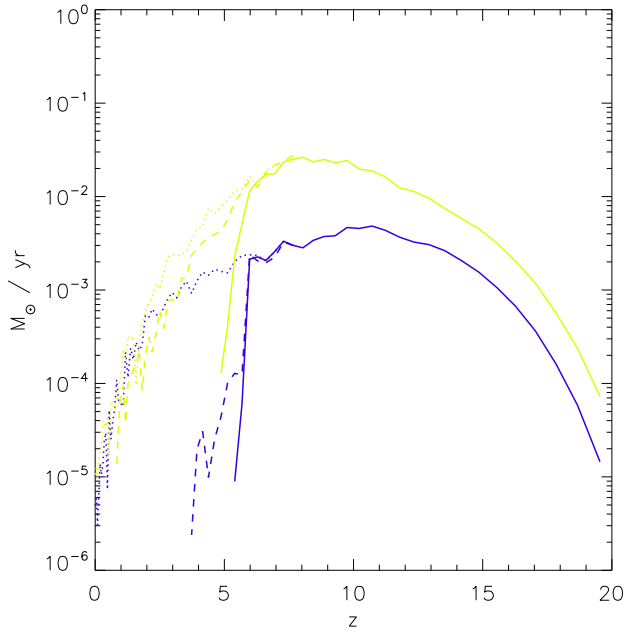

Figure 7. Star formation rate in $M_\odot$ yr^{-1}, for systems of two different masses indicated by the colours, which correspond to those in Figures 5 and 8. All simulations include feedback, and those corresponding to the solid and dashed lines include UV radiation, while those corresponding to the dotted lines do not. The dashed lines also include self-shielding. It can be seen that the star formation rates for systems of a given mass are identical up to redshift $z = 6$. After that, they decline sharply in the scenarios with UV background and no shielding (solid), and much more gradually when the UV background is ignored (dotted). However, the impact of self-shielding (dashed line) is different for the two masses. In the high-mass case, it resembles the case without UV radiation, whereas in the low-mass case, it drops almost as sharply as the one without shielding.

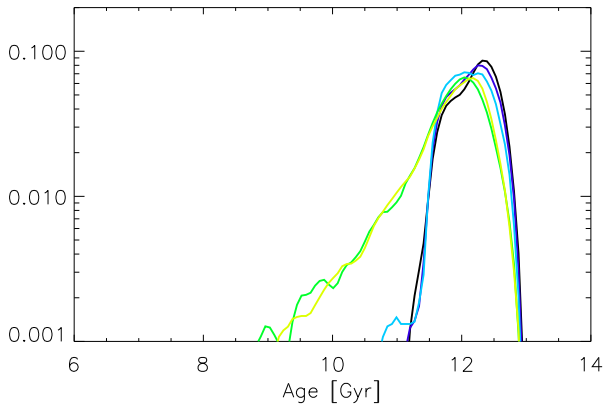

Figure 8. Stellar Ages in Gyr, in simulations with UV background and self-shielding, as described in the text. The colours indicate different masses in the initial conditions, as in Figure 5.

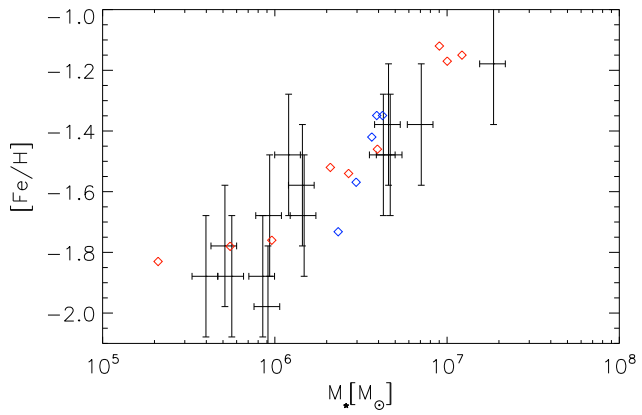

Figure 9. Mean metallicity and stellar mass for 14 observed dwarf spheroidals, in black, together with the results from our simulations. Shown in red is a sequence of simulations (1-9) with varying initial masses, which gives a good fit to the observations. Also shown in blue is a sequence of simulations with varying parameters of $c_\star$. While it intersects with the observed relation, the slope is much too steep compared with observations. The observational uncertainties, as given by Woo et al., are 0.2 dex for [Fe/H] and 0.17 dex for stellar mass.

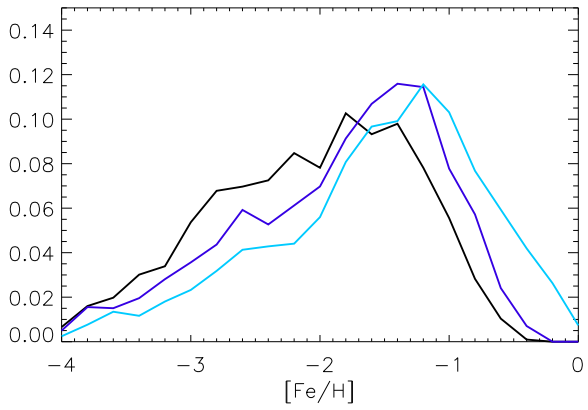

Figure 10. Metallicity distribution of stars for three simulations of different total mass 1 in black, 4 in dark blue and 7 in light blue.

varies by only a factor of two. Strigari et al. also note that for the most luminous dwarf spheroidals such as Fornax, the mass-to-light ratios relating the mass within 300 pc to the total luminosity in the observed galaxies tend to be underestimates, since their stellar populations are typically more extended.

4.2 Star Formation Efficiency

We have also run a number of simulations where we have varied the star-formation parameter $c_\star$, the constant of proportionality that enters the Schmidt law for the rate at which cold gas gets turned into stars. In late-type galaxies, the choice of $c_\star$ has a strong influence on the star formation rate (Ferreras & Silk 2001), and hence the stellar age distri-

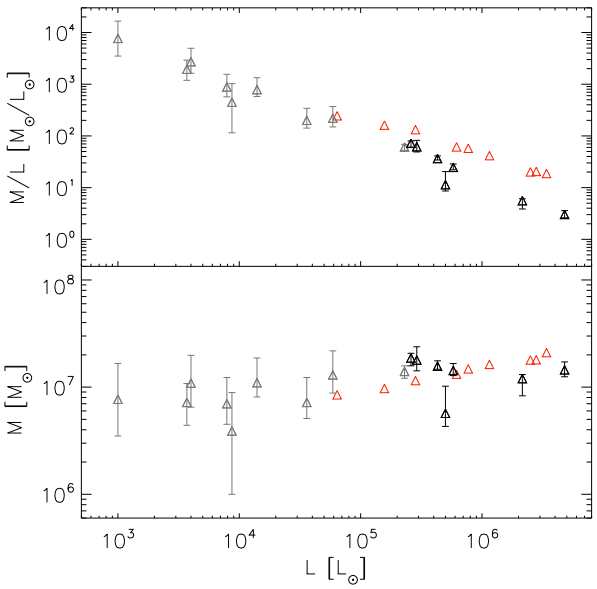

Figure 11. Mass-to-light ratio within 300 pc as a function of total luminosity. Simulations 1 through 9 from Table 1 and which also appear in Figure 9 are shown in red, together with the 8 'classical' Milky Way satellites and the 10 'SDSS Dwarfs' contained in the analysis of Strigari et al., in black and grey, respectively.

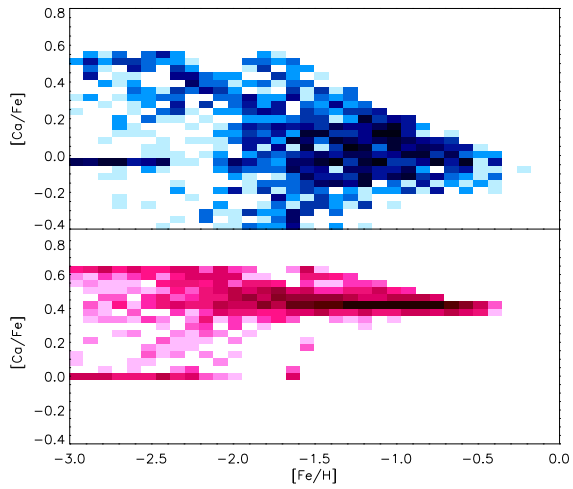

Figure 12. Abundances of [Ca/Fe] vs [Fe/H] of the stars, in simulations with a minimum supernova Ia lifetime of 10^8 years (in blue) and 5×10^8 years (in red).

bution, as well as on the final stellar mass. We find no such strong influence in our dwarf spheroidals. In our simulations, the star formation rate increases with $c_\star$ at all redshifts, and as a result, the final stellar mass scales as roughly $M_\star \propto c_\star^{0.25}$ over the range of $c_\star$ between 0.01 and 0.1, resulting in final stellar masses between 2.3 and $4.2 \times 10^6 \mathrm{M}_\odot$ for a given initial condition corresponding to simulation 4 in Table 1. This relatively weak dependence points to the fact that in dwarf galaxies, the main factor that determines the overall star formation is not the specific efficiency of turning cold gas into stars, but the amount of feedback and UV heating they can sustain before star formation gets shut down, which in our models strongly depends on the depth of the potential well.

There is nevertheless some degeneracy between star formation efficiency and initial mass when it comes to the amount of stars formed. This can be broken partially by considering chemical evolution. In Figure 9 we have included a simulation sequence of differing star formation efficiency but identical initial conditions, plotted in blue, and we compare it to the observed mass-metallicity relation, as well as to the relation obtained from the sequence of simulations with varying total masses. Besides the much narrower range in stellar mass of the $c_\star$ sequence, its slope is also too steep when compared with observations, which in contrast, are well-matched by the varying mass sequence. While the amount of scatter prevents us from selecting a particular value of $c_\star$, it appears that the range in luminosities and the mass-metallicity relation cannot be explained by a simple scaling of the star formation efficiency. For most of our simulations, we have adopted $c_\star = 0.05$, in agreement with Stinson et al. (2007).

4.3 Supernova-progenitor lifetimes

Our feedback model includes both supernovae type II and type Ia. The delay time of supernovae type II is theoretically constrained to be on the scale of Myrs, but due to the uncertain nature of their progenitors, that of supernovae type Ia is much more uncertain. We find that in our simulations, the bulk of the thermal feedback released in time to influence the star formation history is provided by supernovae type II. However, the delay time for supernovae type Ia influences both the total iron enrichment, and the position of the turnover point on the [α/Fe] / [Fe/H] diagram. In dwarf spheroidal galaxies with very short star formation episodes, this effect is particularly strong. We have performed simulations with minimum delay times between 100 Myrs and several Gyrs, and found that once the minimum lifetime is increased above several hundred Myrs, the [α/Fe] ratios are too high, and there is no visible turnover point on the [α/Fe]/[Fe/H] diagram, contrary to the observed distribution of red giants in Local Group dwarf spheroidals (e.g. Shetrone et al. 2003; Tolstoy et al. 2003). The two scenarios are illustrated in Figure 12, which shows the [Ca/Fe] ratios for minimum lifetimes of 10^8 years (in blue) and 5×10^8 years (in red) in two simulations with initial conditions identical to simulation 2 in Table 1 that both have an age-spread of ~ 1.1 Gyrs. With a more careful analysis and better constraints on other aspects of the chemical evolution model, such as the mixing of elements, the initial mass function and the yields, those dwarf spheroidal galaxies which show evidence for enrichment by type Ia supernovae despite an apparently short star-forming phase might therefore provide an upper bound on the minimum lifetime of supernova type Ia progenitors. On the other hand, we are satisfied that allowing the lifetime to be a 'free parameter' of the model, the best fit to the observations is obtained with a minimum lifetime of around 100 Myrs, compatible with the value suggested by Matteucci & Recchi (2001).

4.4 Metal-Enhanced Outflows

Simulations of galaxy formation suffer a generic problem in that thermal feedback from star formation has little effect if it is deposited in nearby gas, since densities are normally so high that the energy is immediately lost to radiation (Katz 1992; Marri & White 2003). Most simulators have fixed this in an ad-hoc way by switching off cooling in the reheated particles for some arbitrary timescale (e.g. Thacker & Crouchman 2000; Governato et al. 2007), or by giving them a kick of arbitrarily specified amplitude (e.g. Navarro & White 1994; Dalla Vecchia & Schaye 2008). Our multiphase treatment of the interstellar medium avoids the need for such ad-hoc fixes but does nevertheless introduce some additional freedom in determining how the energy and metals are shared between the two phases. In the dwarf galaxies we have simulated, most of the ejecta given to the hot phase eventually escape from the system, leaving only those that go to the cold phase to be included in subsequent generations of stars. Thus, increasing the fraction of metals given to the cold phase increases the final metallicity, whereas a high fraction of metals given to the hot phase creates strongly metal-enhanced winds. To some extent, we can use the observed metallicity-luminosity relation of dwarf spheroidals shown in Figure 9 in order to calibrate this parameter. We find relatively good agreement if 25% of the metals and energy are injected to the cold phase. Because this choice effects different elements in the same way, we can use the [Ca/Fe] ratios in order to break the degeneracy between the amount of iron enrichment and the supernova Ia lifetimes.

5 SUMMARY

We have simulated the formation and evolution of dwarf spheroidal galaxies in full cosmological models including supernova feedback and UV radiation. Our models have resulted in dwarf spheroidal galaxies with a wide range in luminosity, 6.4×10^4 to 3.4×10^6 $L_\odot$ and median metallicity, from [Fe/H]$= -1.83$ to -1.12. The variation in total mass, 2.3 to 11.8 $\times 10^6$ $M_\odot$, is surprisingly small, but it is comparable to the values inferred from observations of Local Group dwarf spheroidals. The range of velocity dispersions, 6.5 to 9.7 kms^{-1}, is also in good agreement with the observed range. Our simulations have resulted in two kinds of age distributions, either a single burst of star formation lasting around 1 Gyr, or a burst followed by a tail extending over several Gyrs. Both of these have Local Group analogues. However, in some sense the sample of dwarf spheroidal galaxies in the Local Group is even more diverse. Our limited set of initial conditions did not produce a system as luminous and extended, or with such a large age-spread as Fornax, nor were we able to resolve systems as faint as some of the ultra-faint dwarf galaxies.

We have shown that in our simulations, feedback from supernovae and the cosmic UV background shape both the dynamical and the chemical evolution of dwarf spheroidal galaxies. As a result, these are inseparably linked. We have demonstrated that, with a sensible choice of parameters, the formation of systems comparable to Local Group dwarf spheroidal galaxies is possible. While we stress that we do not suggest that the dwarf spheroidal population in the Local Group reflects merely a variation in halo mass, we conclude that it is possible to reproduce the wide range of observed stellar masses and metallicities, as well as differing star formation histories within a single evolutionary scenario, and for a narrow range of dynamical masses, as observed.

Our simulations put the Local Group dwarf galaxies in a unique position where the gravitational potential is at a critical value with respect to the combined effects of supernova feedback and UV heating. We find that both are necessary to reproduce the observations. In this scenario, a number of dynamical and stellar evolution effects conspire to reproduce the observed scaling relations. More massive galaxies start off with a proportionally higher initial gas mass, and in addition turn a larger fraction of it into stars, because their deeper potential wells moderate supernova-driven outflows and also allow the gas to self-shield against the UV background. On top of that, more efficient recycling of the gas leads to higher metallicities, and a more extended star formation history results in a younger stellar population with higher specific luminosities. While all these effects undoubtedly play a role in the real systems, differing assembly and accretion histories, and differing environments are likely also to influence dwarf spheroidal structure.

With regard to the 'laboratory' characteristics of dwarf spheroidals mentioned in our introduction and underlined by our results, as well as in view of the enormous difference in scale compared with the disk galaxies studied by Scannapieco et al. (2008), the fact that the same dynamical and subgrid models work for both kinds of galaxies is in itself a noteworthy and reassuring result. Our models do not yet include radiative transfer or the mixing of elements in the interstellar medium. In addition, their environment differs from the Local Group, where environmental effects are clearly reflected in relations such as the apparent dependence of star-formation timescale on Galactic distance (van den Bergh 1994; Grebel 1997). Nevertheless, it remains to be seen how important they are compared to feedback and the UV background. Our choice of initial mass function has produced a residual population of metal-free stars in the simulations, which are not observed. The inclusion of early enrichment by Population III stars might remove this discrepancy. Simulations by Wise & Abel (2008) have recently studied how massive Population III stars, and the resulting photoionization at redshifts ~ 30 may affect the interstellar medium in dwarf galaxies. This would be an interesting addition to our models. Addressing these issues should lead to a more complete understanding of the evolution of dwarf galaxies, and should also allow us to make more detailed comparisons with individual objects, exploiting the high quality data that have become available in recent years.

ACKNOWLEDGEMENTS

We would like to thank Volker Springel for his support with the numerical methods that made this work possible, and Adrian Jenkins for his advice and for preparing the initial conditions. We also thank Pascale Jablonka for her advice, which was essential to this and to earlier work. The sim-

ulations were carried out at the computing centre of the Max-Planck Society in Garching.

REFERENCES

Battaglia, G. et al. 2006, A&A, 459,423
Belokurov, V. et al. 2007 ApJ, 654, 897
Bolton, J., Meiksin, A. and White, M. 2004, MNRAS, 348, 43
Bruzual, G. and Charlot, S. 2003, MNRAS, 344, 1000
Carignan, C. and Beaulieu, S. 1989, ApJ, 347, 760
Castellani, M., Marconi, G. and Buonanno, R. 2006, A&A, 310, 715
Chapman, S. C. et al. 2008, ApJ, 662, L79
Ciardi, B., Ferrara, A. and White, S. D. M. 2003, MNRAS, 344, L7
Dalla Vecchia, C. and Schaye, J. 2008, MNRAS, 387, 1431
de Blok, W. J. G., McGaugh, S. S. , Bosma, A. and Rubin, V. C. 2001, ApJ, 552, 23
Dejonghe, H. and Merritt, D. 1992, ApJ, 391, 531
Dekel, A. and Silk, J. 1986, ApJ, 303, 39
Diemand, J., Kuhlen, M. and Madau, P. 2007, ApJ, 667, 859
Efstathiou, G. 1992, MNRAS, 256, 43
Evans, N. W., An, J. and Walker, M. G. 2008, MNRAS, accepted
Faber, S. M. and Lin, D. N. C. 1983, ApJ, 266. 17
Fan, X. Narayanan, V. K. Strauss, M. A. White, R. L. Becker, R. H. Pentericci, L. and Rix, H.-W. 2002, AJ, 123, 1247
Ferrara, A. and Tolstoy, E. 2000, MNRAS, 313, 291
Ferreras, I. and Silk, J. 2001, ApJ, 557,165
Goerdt, T., Moore, B., Read, J. I., Stadel, J. and Zemp, M. 2006, MNRAS, 368, 1073
Governato, F., Willman, B., Mayer, L., Brooks, A., Stinson, G., Valenzuela, O., Wadsley, J. and Quinn, T. 2007, MNRAS, 374, 1479
Grebel, E. K. 1997, Reviews in Modern Astronomy, 10, 29
Grebel, E. K. and Gallagher, III, J. S. 2004, ApJ, 610, L89
Haardt, F. and Madau, P. 1996, ApJ, 461, 20
Hayashi, E. et al. 2003, MNRAS, 355, 794
Helmi, A. et al. 2006, ApJ, 651, L121
Hoeft, M., Yepes, G., Gottlöber, S. and Springel, V. 2006, MNRAS, 371, 401
Hoeft, M., Yepes, G. and Gottlöber, S. 2008, IAU Symposium, 244, 279
Katz, N. 1992, ApJ, 391, 502
Kennicutt, Jr., R. C. 1998, ApJ, 498, 541
Kitayama, T., Tajiri, Y., Umemura, M., Susa, H. and Ikeuchi, S. 2000, MNRAS, 315, L1
Klypin, A., Kravtsov, A. V., Valenzuela, O. and Prada, F. 1999 ApJ, 522, 82
Koch, A.. Grebel, E. K., Wyse, R. F. G., Kleyna, J. T., Wilkinson, M. I., Harbeck, D. R., Gilmore, G. F. and Evans, N. W. 2006, AJ, 131, 895
Koch, A., Kleyna, J. T., Wilkinson, M. I., Grebel, E. K., Gilmore, G. F., Evans, N. W., Wyse, R. F. G., Harbeck, D. R. 2007, AJ, 134, 566
Koch, A., Grebel, E. K., Gilmore, G. F., Wyse, R. F. G., Kleyna, J. T., Harbeck, D. R., Wilkinson, M. I. and Evans, N. W. 2008, AJ, 135, 1580
Lewis, G. F., Ibata, R. A., Chapman, S. C., McConnachie, A., Irwin, M. J., Tolstoy, E. and Tanvir, N. R. 2007, MNRAS, 375, 1364
Li, Y.-S. and Helmi, A. 2008, MNRAS, 385, 1365
Łokas, E. L. 2002, MNRAS, 333, 697
Marlowe, A. T., Heckman, T. M., Wyse, R. F. G. and Schommer, R. 1995, ApJ, 438, 563
Marri, S. and White, S. D. M. 2003, MNRAS, 345, 561
Martin, N. F., Ibata, R. A., Irwin, M. J., Chapman, S., Lewis, G. F., Ferguson, A. M. N., Tanvir, N. and McConnachie, A. W. 2006, MNRAS, 371, 1983
Mateo, M. L. 1998, ARA&A, 36, 435
Mateo, M. and Olszewski, E. W. and Walker, M. G. 2008, ApJ, 675, 201
Matteucci, F. and Recchi, S. 2001, ApJ, 558, 351
Moore, B. 1994, Nature, 370, 629
Moore, B. 1999, ApJ, 524, 19
Nagai, D. and Kravtsov, A. V. 2005, ApJ, 618, 557
Navarro, J. F., Eke, V. R. and Frenk, C. S. 1996, MNRAS, 283, 72
Navarro, J. F., Frenk, C. S. and White, S. D. M. 1997, ApJ, 490, 493
Navarro, J. F. and White, S. D. M. 1994, MNRAS, 267, 401
Read, J. I. and Gilmore, G. 2005, MNRAS, 356, 107
Read, J. I. and Pontzen, A. P. and Viel, M. 2006, MNRAS, 371, 885
Salpeter, E. E. 1955, ApJ, 121, 161
Scannapieco, C., Tissera, P. B., White, S. D. M. and Springel, V. 2005, MNRAS, 364, 552
Scannapieco, C., Tissera, P. B., White, S. D. M. and Springel, V. 2006, MNRAS, 371, 1125
Scannapieco, C., Tissera, P. B., White, S. D. M. and Springel, V. 2008, MNRAS, 389, 1137
Scannapieco, C., White, S. D. M., Springel, V. and Tissera, P. B. 2009, arXiv 0812.0976
Shetrone, M., Venn, K. A., Tolstoy, E., Primas, F., Hill, V. and Kaufer, A. 2003, AJ, 125, 684
Simon, J. D. and Geha, M. 2007, ApJ, 670, 313
Somerville, R. S. 2002, ApJ, 572, 23
Springel, V. 2005, MNRAS, 364, 1105
Springel, V. et al. 2008, MNRAS(submitted)
Stinson, G. S., Quinn, T., Dalcanton, J., Wadsley, J. and Gogarten, S., 2007, Bulletin of the American Astronomical Society, 38, 766
Strigari, L. E., Bullock, J. S., Kaplinghat, M., Simon, J. D., Geha, M., Willman, B. and Walker, M. G. 2008, Nature, 454, 1096
Susa, H. and Umemura, M. 2004, ApJ, 600, 1
Tajiri, Y. and Umemura, M. 1998, ApJ, 502, 59
Thacker, R. J. and Couchman, H. M. P. 2000, ApJ, 545, 728
Tollerud, E. J., Bullock, J. S., Strigari, L. E. and Willman, B. 2008, ApJ, 688, ,277
Tolstoy, E., Venn, K. A., Shetrone, M., Primas, F., Hill, V., Kaufer, A. and Szeifert, T. 2003, AJ, 125, 707
Van den Bergh, S. 1994, ApJ, 428, 617
Van den Bosch, F. C. and Swaters, R. A. 2001, MNRAS, 325, 1017
Thielemann, F. K., Nomoto, K., Hashimoto, M. 1993, in Prantzos N., Vangoni-Flam E., Casse, N., eds, Origin and Evolution of the Elements. Cambridge Univ. Press, Cam-

bridge, p. 299
Valcke, S., de Rijcke, S., Dejonghe, H. 2008, MNRAS, 389, 1111
Walker, M. G., Mateo, M., Olszewski, E. W., Gnedin, O. Y., Wang, X., Sen, B., Woodroofe, M. 2008, ApJ, 667, 53
Walker, M. G., Mateo, M. and Olszewski, E. W. 2009, AJ, 137, 3100
Willman, B. et al. 2005, ApJ, 626, L85
Wise, J. H. and Abel, T. 2008, ApJ684, 1
Wise, J. H. and Abel, T. 2008, ApJ, 685, 40
Woo, J., Courteau, S. and Dekel, A. 2008, MNRAS, online early
Woosley, S. E. and Weaver, T. A. 1995, ApJS, 101, 181